



Age and thermal history of Eo- and Neohimalayan granitoids, eastern Himalaya

Amos B. Aikman^a, T. Mark Harrison^{b,*}, Joerg Hermann^a

^aResearch School of Earth Sciences, Australian National University, Canberra, ACT 0200, Australia

^bDepartment of Earth and Space Sciences, University of California, Los Angeles, CA 90095-1567, USA

ARTICLE INFO

Article history:

Received 19 May 2011

Received in revised form 13 October 2011

Accepted 20 January 2012

Available online 8 March 2012

Keywords:

Tethyan Himalaya

U–Th–Pb

Zircon

Ti thermometry

Eocene magmatism

ABSTRACT

Four distinct granitoid suites outcrop across a N–S transect in the eastern Himalaya between the Main Central Thrust (MCT) and the Indus Tsangpo suture. The Arunachal and Tsona leucogranites outcrop, respectively, in the MCT hanging-wall and adjacent the South Tibetan Detachment. Both crystallized at about 19 Ma, and appear to be lateral equivalents of the High Himalayan Leucogranites. In the central Tethyan Himalaya, the Dala granitoids form a suite of undeformed plutons emplaced into deformed Tethyan Himalayan Sequence metasediments. In the northern Tethyan Himalaya, the Yala-Xiangbo granitoids are part of an igneous complex in the core of the Yala-Xiangbo dome. Both the Dala and Yala-Xiangbo granitoids have Eocene magmatic ages (44.1 ± 1.2 Ma and 42 ± 5 Ma, respectively) that are notably older than the vast majority of post-collisional granitoids along the main Himalayan Arc. Pelitic units from the core of the Yala-Xiangbo dome record two episodes of amphibolite-grade metamorphism and monazite growth coinciding with well-documented episodes of Eohimalayan and Neohimalayan metamorphism. The thermochronological histories of the Dala and Yala-Xiangbo units suggest that the eastern Tethyan Himalaya was tectonically quiescent from ca. 40 Ma until ca. 15 Ma. Miocene exhumation of the Dala and Yala-Xiangbo units, and all North Himalayan Domes studied to date, appears best explained by a structural control, such as concurrent north-directed motion on the Great Counter Thrust. We hypothesize that an extension of the Ninety East Ridge may have been responsible for Eocene high heat-flow beneath the eastern Himalaya and explain the localization of magmatism there.

© 2012 Elsevier Ltd. All rights reserved.

1. Introduction

Understanding the distribution and timing of granitoid magmatism in the Himalaya is akin to knowing the thermal budget within the orogen throughout its history and leads to constraints on the timing of tectonic activity. However, the majority of investigations of Himalayan magmatism (e.g., Le Fort, 1975; Debon et al., 1986; Le Fort et al., 1987; Harris and Massey, 1994; Harrison et al., 1998; Jamieson et al., 2004) have focused on the frontal ranges of northern Nepal and NW India. Most granitoids outcropping in these relatively well-studied regions are Oligo-Miocene leucogranites, leading initially to the view that Tertiary granitoid magmatism along the main Himalayan occurred almost entirely within the past ca. 25 Ma (Le Fort et al., 1987; England et al., 1992; Harris and Massey, 1994; Harrison et al., 1997). These and other factors inspired evolutionary models that largely focused on the Miocene and younger time-period known as the Neohimalayan era. Relatively little is known about magmatism during the formative stages of Himalayan orogenesis at ca. 55 Ma, or indeed the ca. 30 Ma period that followed the Eohimalayan era. Furthermore, comparatively

little is known about the magmatic history of the eastern Himalaya (east of 90°E), although undeformed 44 Ma granitoids have been documented there intruding into highly folded rocks of the Tethyan Himalayan Series (THS) metasediments (Aikman et al., 2008; Zeng et al., 2011).

In this study, we further investigate the distribution and timing of granitic magmatism along a N–S oriented transect through the eastern Himalaya (Fig. 2). We used the Ti-in-zircon thermometer (Watson and Harrison, 2005; Ferry and Watson, 2007) to probe the magmatic and tectonic processes involved in the genesis of these granitoids. Our results confirm that Himalayan granite formation was not confined to the Neohimalayan nor driven solely by fluid-absent melting and that the Eohimalayan history of the eastern Himalaya appears to differ significantly from the rest of the orogen.

2. Geological setting

The Himalaya are the topographic expression of ongoing convergence between the Indian and Eurasian continents since at least the earliest Tertiary (e.g., Yin and Harrison, 2000). Most workers agree that the first-order geology is controlled by a series of predominantly north-dipping regional movement zones that outcrop

* Corresponding author.

E-mail address: tmark.harrison@gmail.com (T.M. Harrison).

sub-parallel to the trace of the Main Himalayan Arc (Fig. 1; Gansser, 1964; Le Fort, 1975; Yin, 2006).

The majority of the Himalayan outcrop is composed of Indian foreland sequences dissected into shear-bounded tectono-metamorphic slices. The highest grade of these units are the Greater Himalayan Crystallines (GHCs), a sequence of paragneisses and migmatitic gneisses exhumed between the reverse sense Main Central Thrust (MCT) and the normal sense South Tibetan Detachment (STD) (Le Fort, 1996). The GHC are in tectonic contact – across the STD – with the overlying, low-grade Tethyan Himalayan Sequences (THSs) metasediments (Burchfield et al., 1992; Le Fort, 1996), the structurally highest and inferred earliest-accreted Himalayan units (Le Fort et al., 1987; Le Fort, 1996; Yin and Harrison, 2000). Both the MCT and the STD were active during the Miocene, but many workers argue their origins date back at least to the Eohimalayan (see Yin and Harrison, 2000). The THS were largely deformed during the Eohimalayan episode (Ratschbacher et al., 1994; Aikman et al., 2008). Deformation of the lower-grade Lesser Himalayan Series (LHS), which outcrop in the MCT-footwall, occurred during the late Miocene and Pliocene (Le Fort, 1996; Yin and Harrison, 2000).

2.1. Himalayan granitoids

Two belts of Himalayan granitoids outcrop sub-parallel to the trace of the main Himalayan Arc (Le Fort, 1975; Le Fort et al., 1987; Le Fort, 1996; Yin and Harrison, 2000). The more southerly High Himalayan Leucogranites (HHL, Fig. 1) form a series of sheet, dyke and laccolithic bodies emplaced into upper parts of the GHC along the crest of the High Himalaya (Le Fort, 1975; Le Fort et al., 1987). They are predominantly muscovite–biotite and muscovite–tourmaline bearing leucogranites that crystallized between 23 and 18 Ma, derived from melting of the underlying pelitic lithologies (Le Fort, 1975; Scharer, 1984; Le Fort et al., 1987; Scharer et al., 1986; Harris and Inger, 1992; Inger and Harris, 1993; Guillot et al., 1994; Harrison et al., 1995, 1997, 1998, 1999), although older episodes have been locally documented (e.g., Prince et al., 2001). Genesis of the HHL has been variously ascribed to shear-heating during movement on the MCT (Harrison et al., 1997, 1998; England

et al., 1992); fluid-present melting associated with overthrusting along the MCT (Le Fort et al., 1987; Prince et al., 2001); decompression-enhanced fluid-absent melting associated with uplift by the MCT and STD (Harris and Massey, 1994); and internal heating from radioactive decay (Nelson et al., 1996; Beaumont et al., 2001).

The North Himalayan Granites (NHGs, Fig. 1) outcrop ca. 80 km to the north of the HHL within the central Tethyan Himalaya. They frequently occur in zones of focused exhumation called the North Himalayan Domes. Most studied NHG crystallized between ca. 10 and 17 Ma but range up to ca. 27 Ma (Chen et al., 1990; Harrison et al., 1997; Lee et al., 2000, 2004; Zhang et al., 2004a,b; Quigley et al., 2006, 2008; King et al., 2011).

Models proposed to account for the NHG include thermal blanketing by the overlying THS metasediments (Pinet and Jaupart, 1987); shear heating along a shallow décollement equated with the MCT (Harrison et al., 1998); decompression melting during extensional collapse (Lee et al., 2004); and high-fluid-phase activity (King et al., 2011) or structural instability in the roof (Beaumont et al., 2004) of an orogenic channel.

3. Sampling and analysis

This study examines four suites of granitoid samples collected along a transect between the MCT and Indus-Tsangpo Suture (ITS), at $\sim 92^\circ\text{E}$ (Fig. 2). The Arunachal leucogranites (Fig. 2) are muscovite–biotite and muscovite–tourmaline bearing leucogranites that form sheet, dyke or laccolithic bodies between the MCT and STD, in frontal regions of the Arunachal Himalaya. They are analogous to the HHL in terms of petrography and emplacement relations (Le Fort et al., 1987; Deniel et al., 1987; Inger and Harris, 1993; Le Fort, 1996; Harrison et al., 1999). Due to access restrictions by military authorities, a suite of similar rocks, the Tsonga leucogranites was collected for us by Dr. Ding Lin from outcrops adjacent to the STD (Fig. 2). Their petrography and emplacement relations appear similar to the Arunachal leucogranites and thus are likely equivalent to the HHL suite, albeit at the highest structural level within the GHCs.

The Dala granitoids are part of an undeformed Eohimalayan (44.1 ± 1.2 Ma) igneous complex emplaced into the deformed

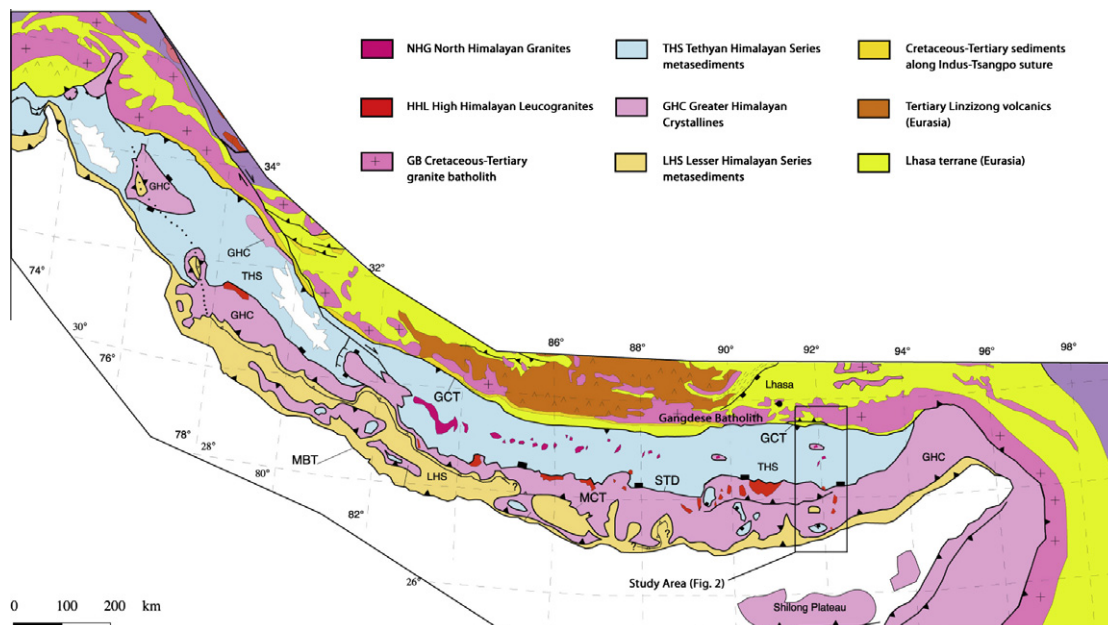


Fig. 1. Regional geological map of the Himalaya (after Yin, 2006). MBT – Main Boundary Thrust; MCT – Main Central Thrust; STD – South Tibetan Detachment; GCT – Great Counter Thrust; red box shows location of Fig. 2. (For interpretation of the references to colour in this figure legend, the reader is referred to the web version of this article.)

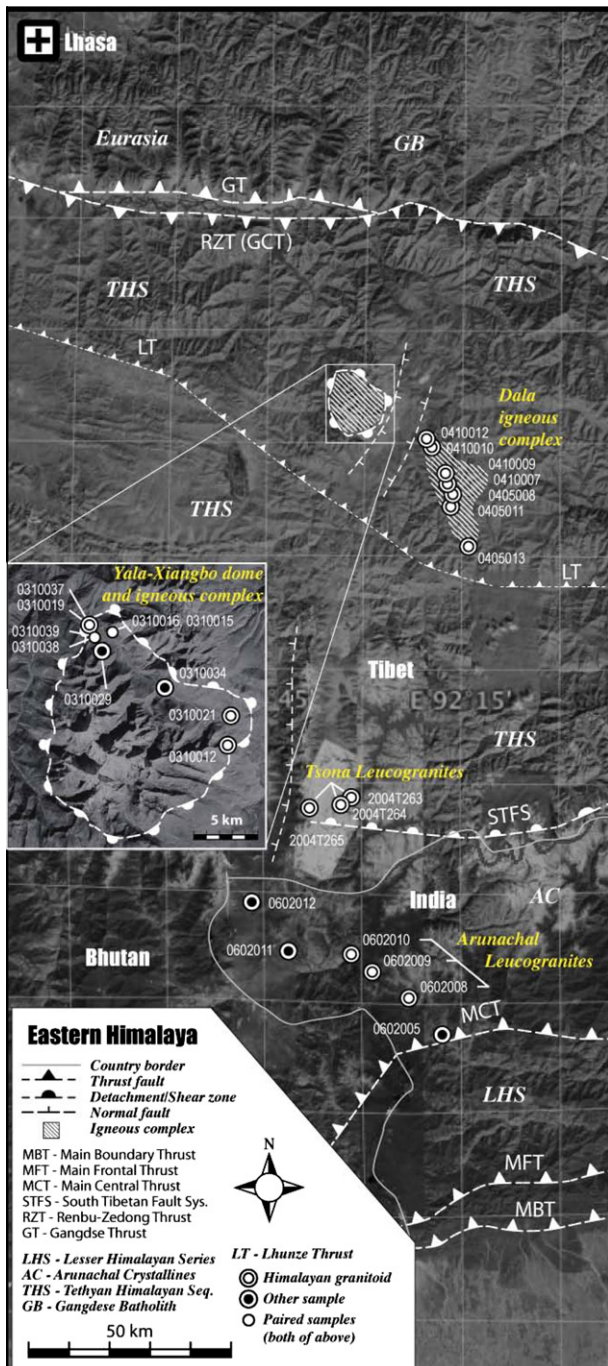


Fig. 2. Simplified geological map of the eastern Himalaya (ca. 92°E), showing key structures and lithotectonic units, and the locations of samples (compiled from Yin et al., 1994; Harrison et al., 2000; Pan et al., 2004; Yin, 2006; Aikman, 2007; this study).

sub-greenschist facies metasediments of the central THS (Fig. 2; Aikman et al., 2008; Zeng et al., 2011). The Yala-Xiangbo granitoids are components of an igneous complex in the core of the Yala-Xiangbo dome (Fig. 2) and are similar to the North Himalayan Granites (NHGs), in terms of emplacement style and structural position (Aikman, 2007). We have also examined several samples of high-grade rocks from the Arunachal crystalline sequence (Fig. 2), and pelitic material from the core of the Yala-Xiangbo dome (Fig. 2), to compare with units cited in the genesis of the HHL and NHG elsewhere.

3.1. Mineral separation and imaging

Mineral separates were obtained using conventional heavy liquid and magnetic separation techniques. We mounted zircons and monazites from the various granitoids in epoxy with reference materials (zircon FC1: 1099.0 ± 0.5 Ma, Paces and Miller, 1993; monazite 554: 45 ± 1 Ma, Harrison et al., 1995), and polished them to expose their midsections, using a rotary polisher and diamond paste. We used optical and electron microscopy, including cathodoluminescence (CL) imaging, to examine the grains for inclusions, cracks and other imperfections (which were avoided during analysis), and to assess their two-dimensional internal structure. Most granitoid zircons ranged from 100 to 500 μm in length, and had subhedral to euhedral morphologies. Monazites from the Yala-Xiangbo granitoid samples were typically subhedral.

3.2. Zircon and monazite U–Th–Pb dating

Zircons and monazites were dated with the SHRIMP RG ion microprobe using U–Th–Pb methods of Williams (1998, zircon) and Harrison et al. (1999, monazite), a 10 kV primary accelerating voltage, a 2–5 nA O_2^- primary-beam current, and a spot size of 12–30 μm diameter. Mass resolving power was ~ 5000 and we used an ion-counting single electron multiplier in peak-hopping mode. No corrections for mass fractionation were made.

Measurements deviating significantly from expected analytical precision were examined for the presence of inclusions and cracks. We reduced the zircon data using the SQUID Excel macro (Ludwig, 2001), with corrections for the sensitivity of Pb relative to U and Th (Paces and Miller, 1993), and zircon standard SL13 (Claoue-Long et al., 1995) to calibrate the absolute U and Th contents of unknowns. Monazite data were reduced using the PRAWN and Lead in-house software packages at ANU. Common Pb was corrected using ^{204}Pb , ^{207}Pb and ^{208}Pb for each analysis and the best choice determined by the method described in Section 4.1. Common Pb corrections assumed the composition of Broken Hill galena (Cumming and Richards, 1975). U–Pb zircon and U–Th–Pb monazite concordia plots are shown in SOM Figs. 1 and 2, respectively and data tabulated in SOM Tables 12–15 (zircon) and SOM Table 16 (monazite).

3.3. Zircon titanium thermometry

The Ti-in-zircon thermometer (Watson and Harrison, 2005; Watson et al., 2006; Ferry and Watson, 2007) provides an empirical framework to estimate the crystallization temperature of zircon by measuring titanium content ([Ti]). In this study, we measured $^{49}\text{Ti}^+$ and $^{28}\text{Si}^{16}\text{O}^+$ using the SHRIMP II in multicollector mode. The primary O_2^- beam current was 4–5 nA, spot sizes ranged from 12–25 μm and analysis points were selected to coincide with U–Th–Pb dating. Analytical precision, based on counting statistics for $\text{SiO}^+/\text{Ti}^+\text{SiO}$ measured in NIST glasses (610, 612 and 615) over the course of an analytical session (24 h), was routinely $\pm 0.2\%$ (ca. 0.1% in NIST 610). Internal precision, based on the standard error of the same ratio measured in SL13 was typically $< 1\%$ but could be as low as 0.5%. We calibrated unknowns against zircon standard SL13 (6.32 ± 0.33 ppm Ti (2σ); Aikman, 2007) which was analyzed once for every 3–5 unknowns. Zircon standard FC1 was used as a secondary reference material to monitor machine drift and reproducibility of the data reduction procedure. In rare cases where the results were anomalous, or deviated significantly from expected analytical precision (typically ≤ 2 analyses per session), we searched for evidence of measurement faults or contamination (e.g., by breaching a Ti-rich crack or inclusion; see Harrison et al., 2007). Ti-in-zircon thermometry results are shown together with U–Pb zircon ages in SOM Tables 12–15.

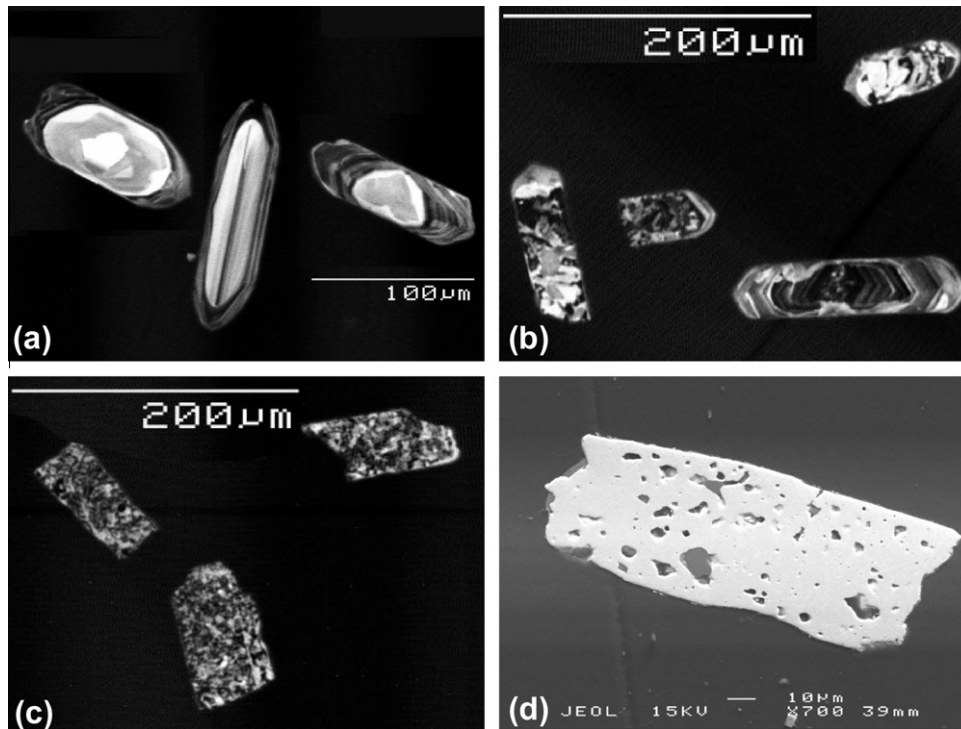


Fig. 3. Electron micrographs (cathodoluminescence and back-scatter) of zircons from the Yala-Xiangbo granitoids: (a) CL image of zircon grains from a sample collected in southern parts of the Yala-Xiangbo igneous complex, showing detrital cores overgrown by relatively pristine igneous rims; (b) CL image of a zircon grain showing anomalous patchy areas cross-cutting concentric zonation; (c) CL image of zircons from northern parts of the complex, showing their spongy texture and tabular habit; (d) back-scatter image a zircon from the same sample as (c), the inclusions are predominantly quartz and feldspar.

3.4. $^{40}\text{Ar}/^{39}\text{Ar}$ dating

Mineral separates, muscovite, biotite and K-feldspar, were obtained Yala-Xiangbo samples using conventional crushing and milling techniques, and irradiated (with Cd shielding) at the HIFAR reactor (Tetley et al., 1980). We analyzed muscovite and K-feldspar by the $^{40}\text{Ar}/^{39}\text{Ar}$ step-heating method, using the ANU VG3600 mass spectrometer and FC-2 sanidine (28.02 Ma; Renne et al., 1998) as a flux monitor. Biotites were analyzed by laser fusion using the same instrument. Data reduction methods followed accepted procedures, described in McDougall and Harrison (1999). Results are shown in Fig. 3 of the SOM and given in SOM Tables 1–11 using the decay constants and ^{40}K abundances recommended by Steiger and Jager (1977) and the correction and J factors given in the table captions.

4. Results

4.1. Internal zircon structures

Arunachal and Tsona zircons show CL patterns characteristic of inherited cores overgrown by concentrically zoned, magmatic rims (Fig. 3a). Yala-Xiangbo granitoid zircons, however, were considerably more variable. Samples from the southern parts of the Yala-Xiangbo complex contained relatively pristine zircons similar to those from the Dala granitoids (Aikman et al., 2008). Samples collected further north, however, often showed patchy textures that cross-cut the concentric zonation (Fig. 3b). In a few samples, virtually all the zircons were mottled and tabular (Fig. 3c), with a spongy appearance under backscattered-electron imaging (Fig. 3d). Zircons from the Yala-Xiangbo high-grade pelites, and one pelitic Arunachal crystalline sample (0602005), showed a range of shapes relative to CL patterns compatible with a detrital

origin. Those from Arunachal crystalline samples 0602011 (meta-granite) and 0602012 (Zhimithang orthogneiss) had igneous CL patterns with thin metamorphic overgrowths (Fig. 3).

4.2. U–Th–Pb dating

The Arunachal and Tsona leucogranites and the Yala-Xiangbo granitoids all contain zircons with Tertiary apparent ages. Most of these ages are concordant (see SOM), and derive from analysis of neofomed igneous rim-domains. The apparent ages from most detrital zircons and restitic zircon cores are also concordant (see SOM); they range from ca. 200 Ma to ca. 3500 Ma for samples outcropping within the THS, or from ca. 450 Ma to ca. 3500 Ma, otherwise.

The best-estimate zircon U–Pb age for each zircon analysis, was calculated according to an automated procedure designed to optimize accuracy and precision while simultaneously minimizing the requirement for qualitative judgments of an individual datum. The best-estimate $^{206}\text{Pb}/^{238}\text{U}$ apparent age was calculated by taking a weighted mean of the ^{204}Pb , ^{207}Pb , and ^{208}Pb corrected values for each analysis. If the MSWD of these 3 ages was found to exceed a critical threshold of 2, the datum was flagged for further evaluation. The accepted age was calculated by taking a weighted mean of the best estimate $^{206}\text{Pb}/^{238}\text{U}$, and the $^{207}\text{Pb}/^{206}\text{Pb}$ apparent ages. However, if the MSWD of these two numbers was found to exceed an empirical threshold of 7, the accepted age was taken as the best estimate $^{206}\text{Pb}/^{238}\text{U}$ age for samples in which the weighted mean of the $^{206}\text{Pb}/^{238}\text{U}$ and $^{207}\text{Pb}/^{206}\text{Pb}$ apparent ages was less than 800 Ma (i.e., the $^{207}\text{Pb}/^{206}\text{Pb}$ age was otherwise used). In cases where the $^{207}\text{Pb}/^{206}\text{Pb}$ apparent age was within error of zero (i.e., young samples with low radiogenic ^{207}Pb content), the $^{207}\text{Pb}/^{206}\text{Pb}$ age was ignored. Thus the approach described above provided a priori rules with which to account for the varying accuracy of the individual

correction methods (especially as a function of age) while ensuring that all were considered in calculation of the final age with minimal need for subjective judgments. $^{208}\text{Pb}/^{232}\text{Th}$ monazite ages were calculated using the ^{207}Pb correction.

Post-analysis imaging of the sampled area for each datum was compared with the CL image to assess overlap on multiple zones potentially leading to mixed ages. Individual measurements were only rejected from the final dataset where several lines of evidence indicated problems. Using this scheme, up to 15% of the measurements from a given analytical session were flagged for detailed consideration, with <5% rejected from the accepted results.

4.2.1. Matrix effects

Himalayan-aged zircons from the Arunachal and Tsona leucogranites and Yala-Xiangbo granitoids have relatively low Th/U ratios (<0.1), but high total [U + Th] contents (up to 40,000 ppm). Variation in the relative sensitivity factors of Pb^+ and U^+ during ion microprobe analysis are well documented (Harrison et al., 1987; Williams and Hergt, 2000; Butera et al., 2001; Hermann et al., 2006). Such “matrix effects” are particularly problematic in zircons containing [U + Th] > 1500–2000 ppm, and can yield positive correlations between [U] or [U + Th] and age in isochronous grains (Williams and Hergt, 2000).

The simplest approach to correcting this effect is to systematically adjust the apparent ages of high [U + Th] grains (>1500–2000 ppm [U]) by a factor proportional to ‘excess’ [U] (i.e., to assume a linear relationship between Pb^+/U^+ ionization yields and U + Th content) (e.g., Williams and Hergt, 2000). We have applied this approach to Himalayan age-populations from the Arunachal and Tsona leucogranites and Yala-Xiangbo granitoids. Data from

the younger growth event in the latter were excluded due to uncertainties in their petrogenesis discussed below, and an insufficient number of analyses to achieve statistical significance. Fig. 4a illustrates the correction applied to the Tsona Granitoids, and Fig. 4b shows corrected and uncorrected age-probability distributions (see SOM for more details of correction methodology).

4.2.2. Age distributions

The distribution of zircon ages within each sample suite as probability density functions (PDF) in Figs. 5 and 6. Data from the rims of Arunachal and Tsona leucogranite zircons cluster into single peaks at ca. 20 and 21 Ma, respectively. Although individual Arunachal leucogranites samples are weakly bimodal (Fig. 5a), it is unlikely this modality is statistically significant at the resolution of the data. Two Tsona leucogranite samples show overlapping age-peaks at ca. 21 Ma; rim ages from the third range from 16 Ma to 26 Ma (Fig. 5b).

Rim ages from the Yala-Xiangbo granitoid zircons form a broad distribution with a dominant peak at 45 Ma, and subordinate peaks at ca. 25 and 20 Ma (Fig. 5c). However, closer examination shows these samples are divisible into two modes: Eocene ages come from zircons (or parts thereof) with relatively pristine, concentric CL zonation (Fig. 3a); whereas Miocene ages are exclusively derived from anomalous, patchy grains or areas (e.g., Fig. 3c). Samples containing both Eocene and Miocene ages show transitional CL patterns (e.g., Fig. 3b).

Monazites separated from the Yala-Xiangbo granitoids, and one sample of the Yala-Xiangbo pelites, show a similar distribution of Himalayan ages, with peaks respectively at ca. 18 Ma and 40 Ma (Fig. 5d). The $^{206}\text{Pb}/^{238}\text{U}$ ages from the older group are somewhat more scattered and younger than their associated $^{208}\text{Pb}/^{232}\text{Th}$ ages (see SOM), which may reflect formation of U-rich exsolution lamellae (Harrison et al., 2002) during the younger monazite growth event.

Most zircon ages from the Yala-Xiangbo pelites are in the range 200 to 1200 Ma. The youngest (ca. 200 Ma) come from samples collected at shallower structural levels, whereas zircons from structurally deeper samples are typically 450 Ma or older (Fig. 6a). Detrital zircon ages from the pelitic Arunachal sample range from ca. 700 Ma to ca. 1800 Ma (Fig. 6b); those from the two meta-granitic samples (meta-granite 0602011 and Zhimithang Gneiss 0602012) cluster at ca. 824 Ma (Fig. 6b).

Age populations from the inherited cores of Yala-Xiangbo granitoids and Arunachal leucogranites zircons are comparable to those of their host lithologies, at the resolution of the data (Fig. 5c–e). We do not have samples of the host lithologies, but the range of Tsona leucogranite core-domain ages (Fig. 5d) is similar to detrital samples from the THS (Aikman et al., 2008).

4.3. Zircon titanium thermometry

The Ti-in-zircon thermometer is a function of temperature, a_{SiO_2} and a_{TiO_2} (Ferry and Watson, 2007). In rocks of broadly granitic composition, a_{SiO_2} is typically close to unity. By using thin-section optical petrography (transmitted and reflected) and examining mineral separates in a binocular microscope, we found that ilmenite is the principal Ti-bearing phase in the Dala granitoids, whereas all other granitic samples contain rutile. Ilmenite implies an a_{TiO_2} of approximately 0.5–0.6; hence the Dala zircon apparent temperatures may underestimate their true values by up to ca. 50 °C (Watson and Harrison, 2005). The presence of rutile implies a_{TiO_2} close to unity, such that the apparent temperatures in the remaining samples likely approximate their true values. This interpretation assumes that zircon co-crystallized with a Ti-rich phase throughout the magmatic episode. We also caution that these buffering assemblages pertain only to the most recent magmatic episode;

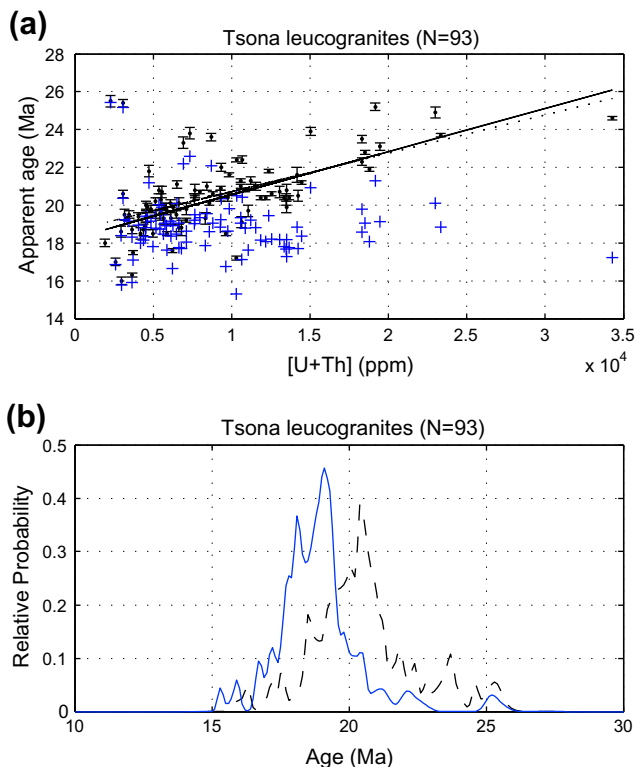


Fig. 4. Plots illustrating the matrix correction applied to the Tsona leucogranites (other suites treated similarly, as discussed in the text). (a) Variation of age with total [U + Th]. Original data shown in black, with error bars; corrected data shown in blue. Solid and dotted lines are, respectively, robust and least-squares regressions to the data. (b) Age probability density functions calculated for the original (black) and corrected (blue) data. (For interpretation of the references to colour in this figure legend, the reader is referred to the web version of this article.)

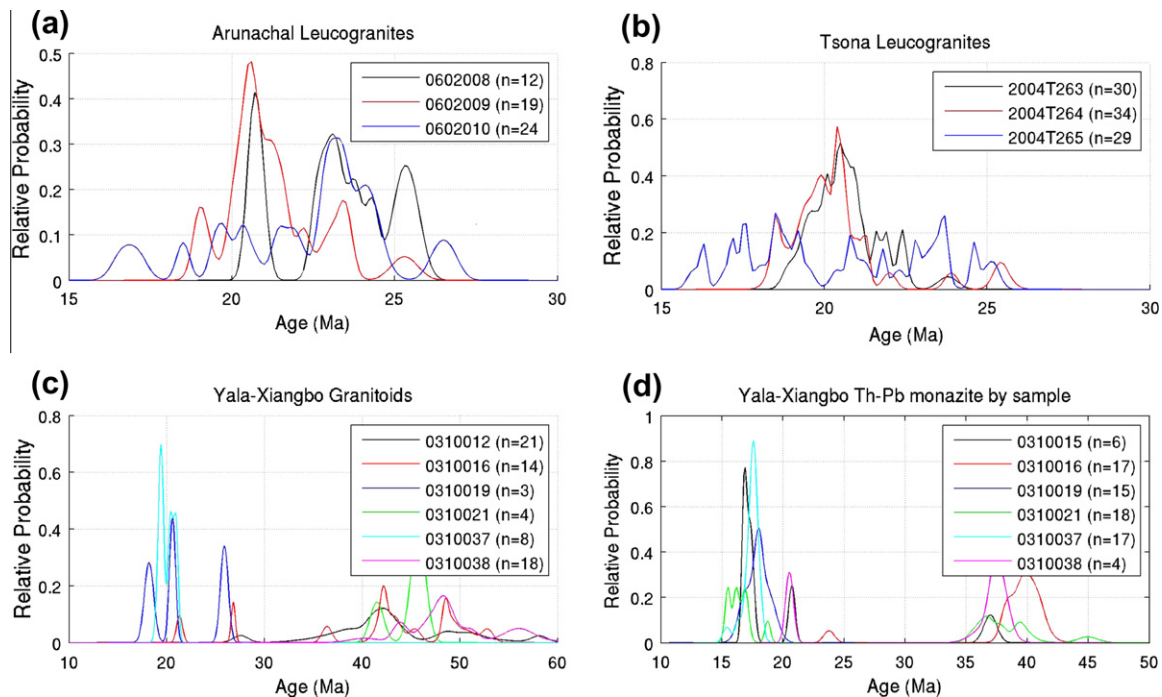


Fig. 5. U–Th–Pb age–probability plots for the rim domains of (a) Arunachal leucogranite zircons; (b) Tsona leucogranite zircons; (c) Yala-Xiangbo granitoid zircons; (d) Yala-Xiangbo monazites. Data shown separated by rock sample and are not matrix-corrected.

the a_{TiO_2} and a_{SiO_2} of inherited and detrital grains are unconstrained, and hence add an additional unknown uncertainty to these data.

Probability density functions of crystallization temperatures of zircons with Himalayan ages are shown in Fig. 7a for all granitoid suites (data tabulated in SOM). The Arunachal and Tsona leucogranites show offset peaks at ca. 660 °C and 730 °C, respectively, although there is a small shoulder on the Arunachal leucogranite peak that coincides with the main Tsona leucogranite peak. The dominant temperature peaks in the Arunachal leucogranites samples (Fig. 7b) increases, from ca. 640 °C to ca. 700 °C, proportional to increasing structural height (Fig. 2). Tsona sample 2004T263 has a single dominant peak at ca. 750 °C (Fig. 7c), whereas Tsona sample 2004T264 has smaller peaks at ca. 750 °C and ca. 550 °C (Fig. 7c). The temperature distribution from Tsona leucogranite sample 2004T265 is broader, ranging from ca. 800 to 550 °C (Fig. 7c). The Dala granitoid Himalayan-aged zircon temperature distribution is strongly asymmetrical, skewed to higher temperatures (Fig. 7a), with little significant difference among samples. All Yala-Xiangbo zircon temperatures derive from a single sample (0310038), in which zircon grains show large areas of anomalous CL patterns. These data form a broad peak below 600 °C (see below for discussion) whose width is significantly enhanced by large analytical uncertainties on measurements of such low [Ti] grains.

The temperature distribution from a combined subset of all the pre-Himalayan (>65 Ma) data is a broad peak centered close to 700 °C. Temperature distributions from the Yala-Xiangbo pelites and Arunachal crystalline samples (0602005 Arunachal GHC and 0602012 Zhimithang Gneiss) are similar to those of the inherited grains from the magmatic samples; the distribution from sample 0602011 (Arunachal meta-granite) is a tight peak centered at 710 °C.

4.4. Zircon petrogenesis

Several samples, in particular the Yala-Xiangbo sample, contain zircons with Ti temperatures that fall below the “wet” granite

solidus. In order to better understand the origin of these zircons and temperatures, we have investigated correlations between age, temperature and trace element (Th, U) systematics.

In the simple case of monotonic cooling of single granitic body, zircon ages and crystallization temperatures should decrease concomitantly, and zircon [U,Th] be governed by partition coefficients and the availability of these elements in the adjacent melt. However, data from the Arunachal and Tsona leucogranites and Dala granitoid zircon rims (Fig. 8) do not show an obvious correlation between age and temperature (or temperature and [U]), and only a weak correlation between Th/U ratio and age. These findings could reflect natural phenomena, such as magma recharge and/or temperature fluctuations (e.g., Claiborne et al., 2006, 2010) but since we cannot rule out analytical problems due to matrix effects, we have also collected data along transects parallel to growth-direction within individual zircon grains, as a proxy for age.

Most zircon grains record a general core-to-rim decrease in temperature, age and Th/U ratio, but these trends are not necessarily either monotonic or smooth; in many cases, they appear correlative with the style of CL zonation. Grains displaying near uniform appearance under both optical and electron imaging usually have the most uniform temperature and trace element patterns. Oscillatory zoned zircons typically show a general core-to-rim decrease in temperature and Th/U ratio, but may display significant variability between CL zones. Grains with longitudinal CL zonation usually record similar temperatures and Th/U ratios along the length of individual zones. In virtually all cases, however, sub-grains or areas of patchy, cross-cutting CL zonation record anomalously low temperatures (sometimes sub-solidus temperatures), low Th/U ratios and younger ages.

The grain shown in Fig. 9 is representative of our combined observations from several dozen others. Its CL pattern indicates a restitic core overgrown by concentrically zoned rim, which is itself cross-cut by areas of patchy, anomalous zonation. Nine analysis spots provide a tip-to-tip transect through all three CL domains. The apparent age of the core domain is ca. 400 Ma, confirming its inferred restitic origin. Ages from the concentrically-zoned rim

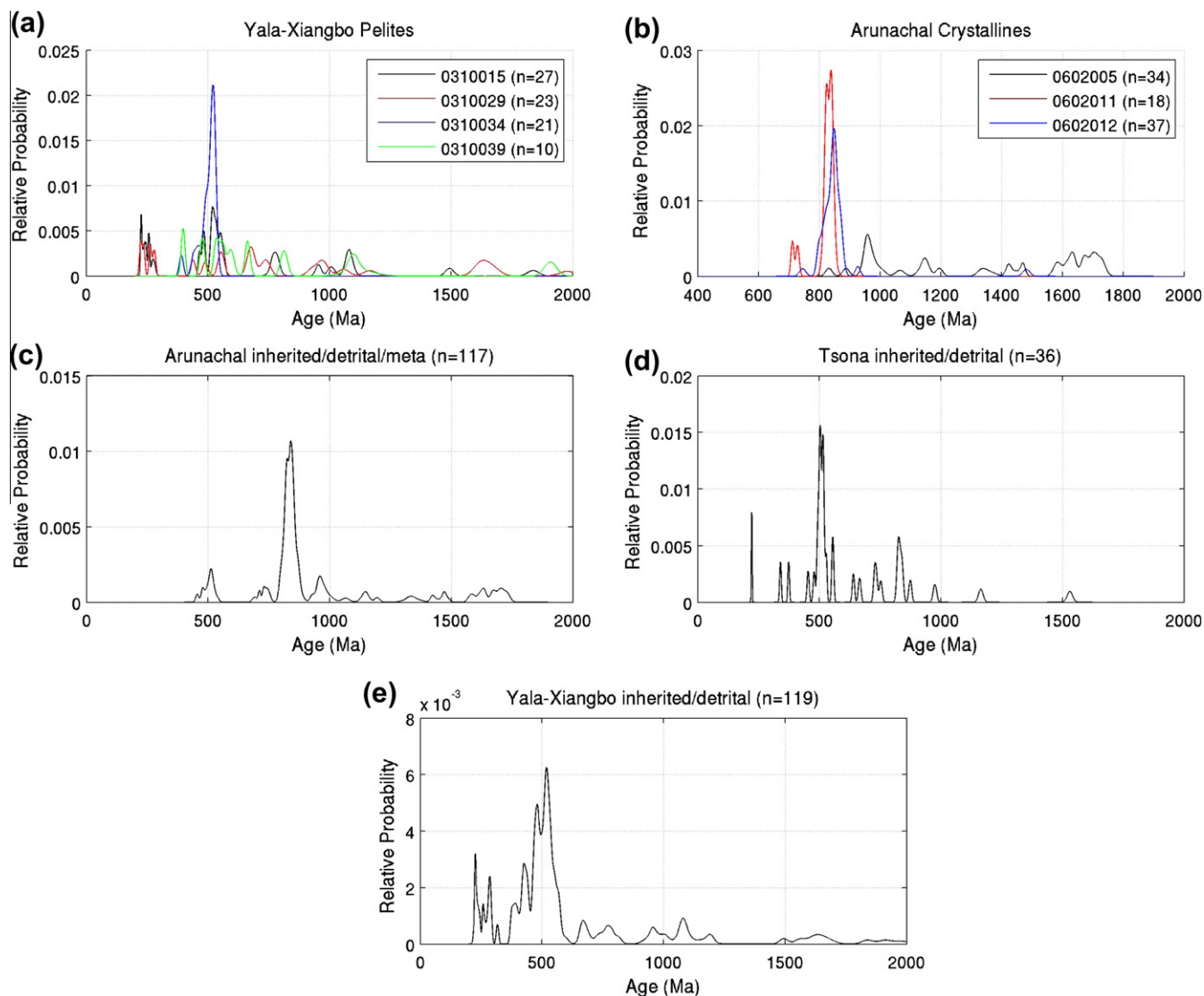


Fig. 6. U–Pb age-probability plots for zircons from the (a) Yala-Xiangbo pelites; (b) Arunachal crystallines; (c) inherited core of zircons from Arunachal leucogranites; (d) inherited cores of zircons from the Tsona leucogranites; (e) inherited cores of zircons from the Yala-Xiangbo granitoids.

domains are consistently ca. 21 Ma, decreasing slightly towards the grain tips, as do crystallization temperature and Th/U ratio. The areas of anomalous, patchy zonation record notably younger ages (ca. 17 Ma), lower Th/U ratios and temperatures that fall below the “wet” granite solidus (e.g., Huang and Wyllie, 1986). Based on similar observations across several sample suites, we conclude that anomalous CL-patterns and sub-solidus Ti temperatures reflect recrystallization, probably associated with late- or post-magmatic fluids. Although the ages from these anomalous zones are consistently younger than those from pristine areas, data resolution is insufficient to reliably date the recrystallization event other than providing a lower bound of ≥ 16 Ma.

4.5. $^{40}\text{Ar}/^{39}\text{Ar}$ thermochronology

Age spectra from the muscovite and K-feldspar samples are relatively flat, with little or no evidence of excess $^{40}\text{Ar}^*$ contamination (McDougall and Harrison, 1999). Most mica total fusion ages are close to 13 Ma; the K-feldspar total fusion is ca. 12 Ma. The thermal history from the K-feldspar sample, recovered using the Multiple diffusion domain (MDD) model (Lovera et al., 1989), indicates rapid cooling at ca. 12 Ma, consistent with the form of the mica

age spectra and the total fusion ages. Thus, our data record rapid mid-Miocene cooling Yala-Xiangbo complex (Fig. 10).

We did not investigate the sub-solidus thermal histories of the Arunachal and Tsona samples, but similar units in the central Himalaya passed through the muscovite K–Ar closure window (ca. 400 °C; Harrison et al., 2009) during the Miocene.

5. Regional implications

5.1. Himalayan magmatism

At least four suites of Tertiary granitoids outcrop in our eastern Himalayan transect between the ITS and the MCT. U–Th–Pb analyses of neo-formed igneous zircon-rims yield concordant ages that date crystallization. Both the Tsona leucogranites and Dala granitoids are emplaced into relatively lower-grade units (Aikman et al., 2008; Aikman, 2007) and thus emplacement and crystallization likely occurred over a short ($<10^5$ years) timescale. The Arunachal leucogranites and Yala-Xiangbo granitoids outcrop within units that experienced upper-amphibolite facies metamorphism.

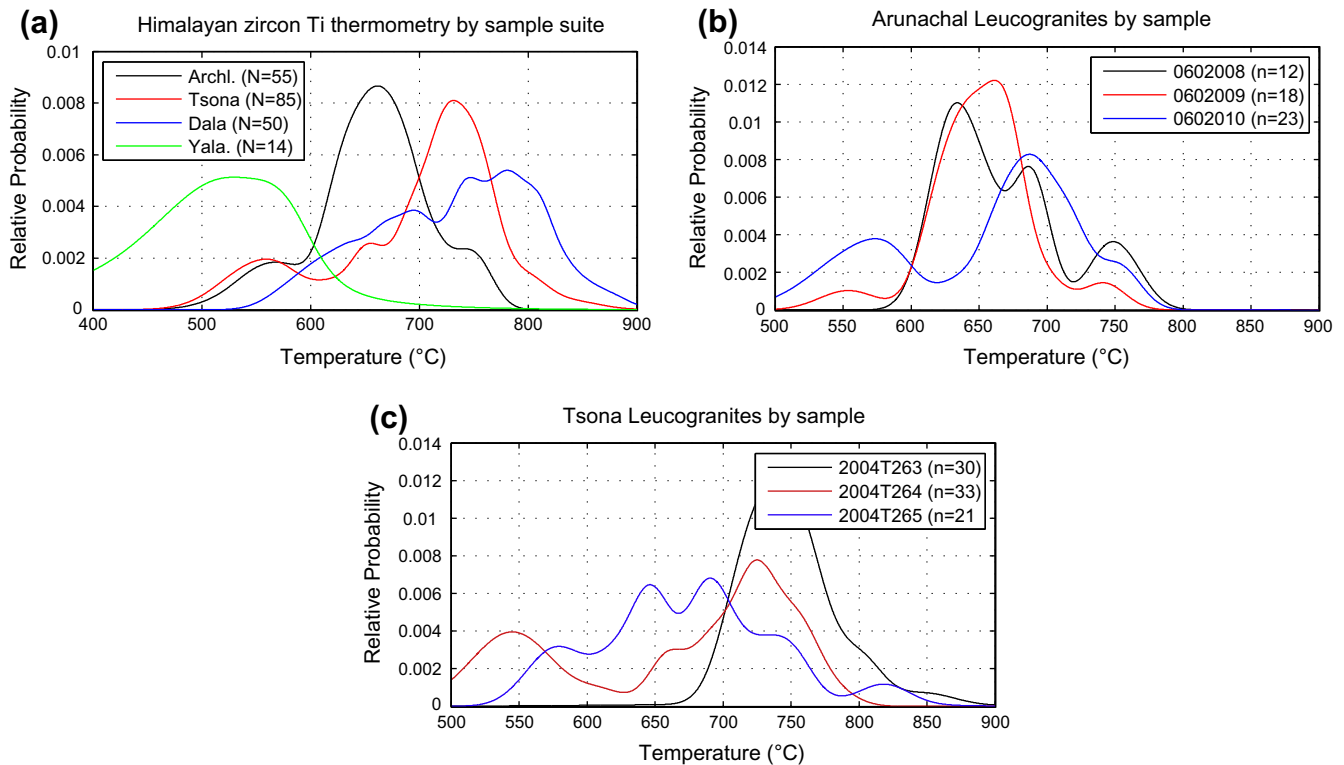


Fig. 7. Ti-in-zircon temperature probability plots for: (a) Himalayan-age zircons, separated by suite (Dala granitoid suite not corrected for a_{TiO_2} , see text for discussion); (b) Arunachal leucogranites, separated by sample; (c) Tsona leucogranites, separated by sample.

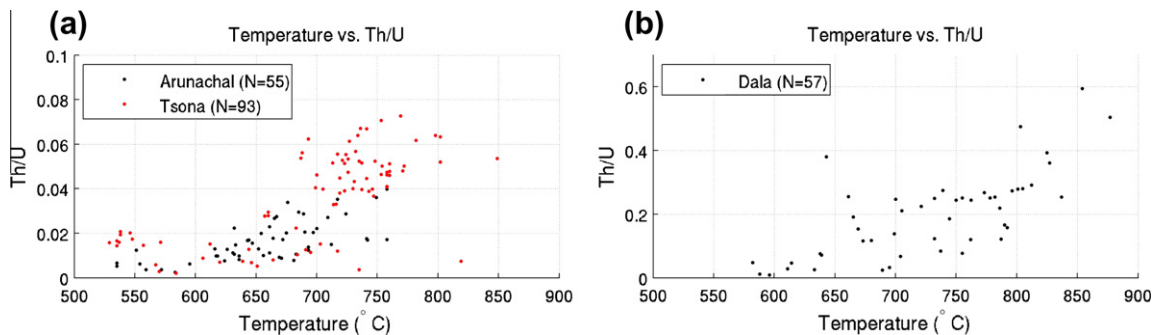


Fig. 8. Graphs showing positive correlation between crystallization temperature and Th/U ratio for (a) Arunachal and Tsona leucogranites, (b) Dala granitoids. Correlations are statistically significant at the 1% level based on Spearman's rank coefficient (Press et al., 1992).

We interpret the median and standard error of U–Pb ages from neo-formed zircon rims of the Arunachal (20.2 ± 2.0 Ma) and Tsona (18.8 ± 1.2 Ma) leucogranites to be crystallization ages. The Dala granitoids crystallized at 44.1 ± 1.2 Ma (Aikman et al., 2008). Most Yala-Xiangbo granitoid zircon ages form a broad peak centered at ca. 42 Ma, but there is also a secondary peak at ca. 20 Ma. Data forming the younger peak derive almost exclusively from zircons (or parts thereof) showing anomalous CL patterns, low Th/U ratios and apparent near- or sub-solidus temperatures that we believe to be associated with recrystallization. Therefore, we interpret the Yala-Xiangbo granitoid age as the median and standard error of data from pristine areas that form the older peak (42 ± 5 Ma). This interpretation is consistent with the absence of Eocene-aged monazite in samples yielding only Miocene zircon ages (because monazite is generally more soluble than zircon in low-pH aqueous fluids; Ayers and Watson, 1991; Townsend et al., 2000).

The Arunachal and Tsona leucogranites crystallization ages are similar to many other HHL (Scharer, 1984; Scharer et al., 1986;

Deniel et al., 1987; Copeland et al., 1990; Edwards and Harrison, 1997) supporting our inferred strike-parallel extension of the HHL suite into the eastern Himalaya. The Yala-Xiangbo granitoid crystallization age is within error of the age of the Dala granitoids (44.1 ± 1.2 Ma; Aikman et al., 2008; Zeng et al., 2011), which outcrop ca. 60 km farther south. We interpret the bimodal distribution of monazite ages in Yala-Xiangbo granitoids and Yala-Xiangbo pelite samples as recording two episodes of Himalayan amphibolite-grade metamorphism (Harrison et al., 2002). The ages of these events coincide with the Eohimalayan and Neohimalayan metamorphic episodes (Le Fort, 1996). Thus, our data show that North Himalayan granitoid magmatism in the eastern Himalaya began within 10–15 Ma of the initiation of Himalayan collision (Yin and Harrison, 2000). Even the earliest Eocene magmatism was intimately associated with high-grade metamorphism, and magmatism continued, at least sporadically, for more than half of the orogen's history. The existence of Eohimalayan plutons and anatectic leucogranites is particularly challenging for existing Himalayan

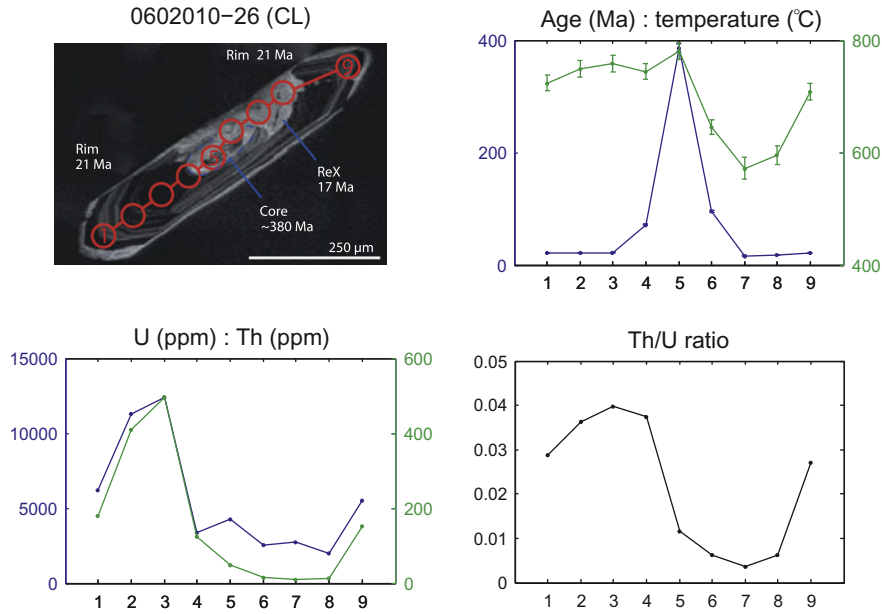


Fig. 9. Core-to-rim ion microprobe transect showing trends in age, crystallization temperature and trace element systematics for grain 0602010-26 from the Arunachal Leucogranites.

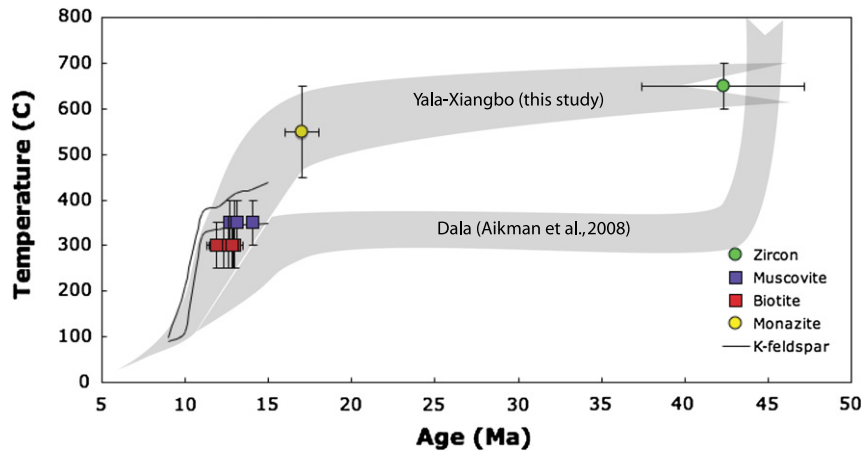


Fig. 10. Thermal histories of the Yala-Xiangbo granitoids (this study) and the Dala granitoids (Aikman et al., 2008). Thermal histories inferred from zircon and monazite U–Th–Pb dating, saturation thermometry and $^{40}\text{Ar}/^{39}\text{Ar}$ thermochronology.

evolutionary models, the majority of which lack a convincing heat source to account for Eohimalayan high-temperature metamorphism.

5.2. Thermal history

Fig. 10 shows the thermal histories of the Dala granitoids (Aikman et al., 2008) and Yala-Xiangbo dome, as reconstructed from zircon and monazite U–Th–Pb dating and saturation thermometry (Aikman, 2007), and $^{40}\text{Ar}/^{39}\text{Ar}$ thermochronology. Crystallization of the undeformed Dala granitoids marks the cessation of regional crustal thickening in the Tethyan Himalaya (Aikman et al., 2008; Zeng et al., 2011), and, presumably, the onset or continuation of shortening farther south. Both the Dala and Yala-Xiangbo granitoids appear to remain broadly isothermal from ca. 40 Ma until their rapid exhumation at ca. 15 Ma. Because Eocene mica and Miocene K-feldspar ages constrain the Dala granitoids to a narrow thermal window, the eastern Tethyan Himalaya was probably tectonically quiescent during this time period.

Miocene exhumation of the Dala igneous complex and Yala-Xiangbo dome occurred concurrently with the exhumation of almost all North Himalayan Domes studied to date (e.g., Lee et al., 2000, 2004; Zhang et al., 2004a,b; King et al., 2011). This remarkable coincidence over several 100 kms along strike, including exhumation of the Yala-Xiangbo complex, argues strongly for a structural control. The simplest mechanism to explain this cooling is Miocene north-directed motion on the Great Counter Thrust (GCT; Yin and Harrison, 2000). This is consistent with the observation of King et al. (2011) who found that North Himalayan Dome granitoids to the west were emplaced before initiation of top-to-north shearing thus constraining GCT activity to post-date ca. 23 Ma.

5.3. Detrital zircon provenance

The distribution of detrital zircon U–Pb ages from structurally higher Yala-Xiangbo pelite samples is very similar to that found in the surrounding uppermost Triassic THS metasediments

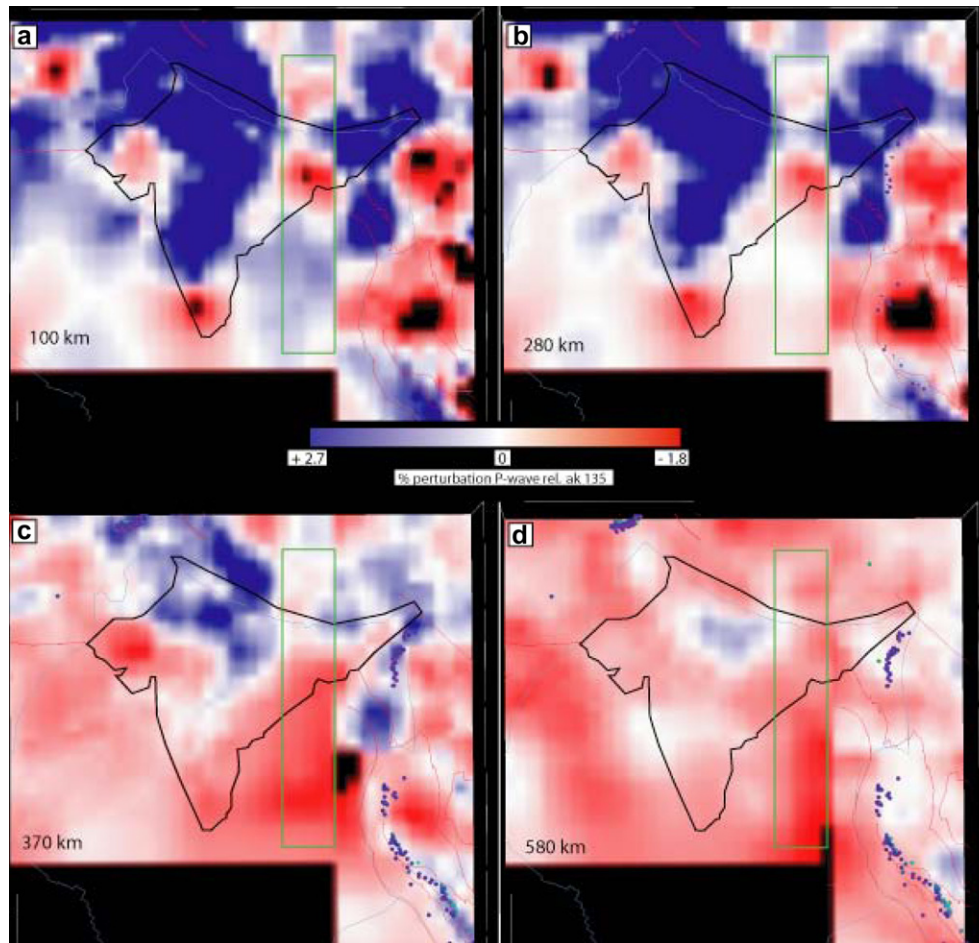


Fig. 11. Horizontal contoured sections through *P*-wave tomographic data. Blue indicates fast wave-speed perturbations and red indicates slow perturbations, from the ak135 model of Kennett et al. (1998) for 100, 280, 370, and 580 km depths. There is a slower-than-average wave-speed anomaly (green box), likely due to higher temperatures, close to the landward projection of the Ninety East bathometric ridge (figure courtesy of Dr. S. Richards). (For interpretation of the references to colour in this figure legend, the reader is referred to the web version of this article.)

(Aikman et al., 2008), whereas in samples from deeper structural levels, we found only Ordovician and older grains (>450 Ma). This supports the preservation of Paleozoic sequences in the core of the Yala-Xiangbo dome (inferred from paleontological evidence; e.g., Pan et al., 2004), similar to those found in the Kangmar Dome farther west (Lee et al., 2000). These Paleozoic units may represent the basement to the THS, exhumed beneath a regional shear-zone that joins the STD to the south with the Great Counter Thrust to the north (Yin, 2006). However, our data do not support a direct correlation between this basement and the GHC proper (e.g., distribution shown in Gehrels et al., 2003), or with the Arunachal crystalline samples.

Based on their detrital zircon age distributions, the three Arunachal crystalline samples are not directly correlative with the central Himalayan GHC. While the pelitic sample (0602005) from the base of the Arunachal crystalline sequence is plausibly similar to pre-Ordovician units found in central Nepal (e.g., Gehrels et al., 2003), both granitic samples (0602011 and 0602012) contain abundant ca. 800 Ma grains (Fig. 6b) that are uncharacteristic of the GHC as defined in Nepal (Le Fort, 1996; Yin and Harrison, 2000; Myrow et al., 2003; Gehrels et al., 2003). Although isolated ca. 800 Ma granitoids (e.g., 823 ± 5 Ma Chor Granite; Singh, 2003) have been documented in the MCT hanging wall elsewhere, Yin (2006) argued that this part of the Arunachal crystalline sequence is correlative with Indian basement lithologies exposed in the Shillong Plateau, thus implying that crustal shortening in the

Arunachal Himalaya included thick-skinned deformation (cf. DeCelles et al., 2001a; DeCelles et al., 2001b). Our results broadly support this conclusion.

5.4. Granitoid provenance

The distribution of ages from Arunachal leucogranites core domains includes ca. 800 Ma grains that support partial melting or assimilation of Arunachal crystalline material. The Tsona leucogranite and Yala-Xiangbo inherited grains include ages as young as ca. 200 Ma, which are almost certainly from THS grains. Therefore, all our leucogranite samples are consistent with partial melting or assimilation of nearby lithologies.

For water contents applicable to most granitic magmas, zircon dissolution is fast with respect to the time scales of melt formation (Harrison and Watson, 1983; Watson, 1996). Therefore, it is reasonable to assume that the Arunachal and Tsona leucogranites magmas were essentially incapable of dissolving any more Zr at their peak temperatures. Zr-saturated magmas should crystallize zircon once temperature begins to decrease, because the solubility of Zr in granitic melts varies exponentially with temperature (Watson and Harrison, 1983). So, in the case of zircon-saturated anatectic melts subject to monotonic cooling, the largest Ti-temperature peak should lie at the upper end of the temperature spectrum (Harrison et al., 2007) and closely approximates the peak melting temperature. The crystallization sequence will only significantly

affect the form of the Ti-temperature distribution in the latter stages of crystallization, when the [Zr] content of the magma (and hence its capacity to crystallize zircon) has been reduced. The Tsona leucogranite distribution is a single peak at the upper-end of the temperature spectrum (ca. 730 °C). Therefore, we attribute their origin to vapor-absent muscovite melting, followed by emplacement and relatively rapid crystallization close to the STD.

The Ti-temperature distribution of the Yala-Xiangbo granitoid zircons lies well below the muscovite fluid-absent melting reaction. Even though the width of the peak is significantly enhanced by the large analytical uncertainties (due to low [Ti]), it is nevertheless clear that most measurements fall below the “wet” granitoid solidus. We interpret these data to reflect recrystallization rather than magmatic temperatures, consistent with other lines of evidence described above.

The Arunachal leucogranites show a broader temperature distribution with the dominant peak at ca. 660 °C, and a small shoulder at ca. 730 °C. This pattern could be interpreted to reflect “wet” melting, a hypothesis that will be explored in detail in a later contribution.

5.5. Eocene heat source

Perhaps the most challenging aspect of the magmatic history of our eastern Himalayan transect is explaining the appearance of a N–S belt of peraluminous granitoids south of the ITS shortly after initiation of Indo-Asian collision. It has been suggested (e.g., Zeng et al., 2011) that asthenospheric upwelling induced by Neo-Tethyan slab break-off (e.g., Davis and von Blanckenburg, 1995) could have resulted in the impingement of hot materials at the base of the Tethyan Himalayan crust with concomitant melting of garnet–amphibolite lithologies. However, volcanic products associated with this event north of the ITS (i.e., Linzizong volcanics) are dominantly 64–61 Ma andesites distributed across the arc (Pan et al., 2004), although the thin upper rhyolitic formation does get as young as 44 Ma (Mo et al., 2008). South of the ITS, documentation of ca. 44 Ma granitoids is restricted to a small intrusion into an ophiolitic mélange within the ITS zone (Pullen et al., 2011) and an undeformed leucogranite in an equivalent structural position to Dala at ~85°E (Ding et al., 2005). Thus the appearance of Eocene peraluminous magmatic rocks at multiple locations along a N–S transect at ca. 92°E may suggest a heat source uniquely confined to the Eastern Tethyan Himalaya.

Tomographic inversions reveal a slow seismic velocity anomaly beneath the eastern Himalaya (Fig. 11). This zone is characterized by velocity perturbations similar to those observed beneath the Deccan Traps and eastern Australia, and attributed to locally elevated mantle temperatures (Kennett and Widiyantoro, 1999; Simons et al., 1999). The anomaly coincides with the termination of the Ninety East Ridge (NER), which extends along the 90°E parallel, from the central Indian Ocean into the Bay of Bengal (Fig. 10). The Ninety East Ridge is the surface expression of a persistent lithospheric discontinuity which we hypothesize may have localized magmatism and heat-flow beneath the eastern Himalaya during the Eohimalayan period. This scenario explains the presence of peraluminous rocks south of the ITS (in the form of the Dala granitoids mafic component), and the mafic sills found at deeper structural levels within the Yala-Xiangbo dome (Aikman, 2007). The NER may also have localized Tertiary arc-magmatism in the eastern Gangdese Batholith, which was especially active during the Eocene (Mo et al., 2006; Pan et al., 2004), directly north of the Dala granitoids.

Presently, high heat flow in southern Tibet (up to 146 mW m⁻²; Francheteau et al., 1984) is restricted to N–S rifts, particularly the Yadong–Gulu rift, with limited measurements in the vicinity of our transect indicating a much lower heat flux of 60–70 mW m⁻²

(Wang, 2000, 2001; Hu et al., 2000). If our supposition regarding the 90°E ridge as Eocene heat source is correct, the subsequent ca. 40 m.y. of underthrusting of the Indian plate would likely have returned the local crust to the more subdued thermal structure characterized elsewhere across the arc.

6. Conclusions

Four suites of Himalayan granitoids are documented along a N–S transect through the eastern Himalaya at ca. 92°E. The Arunachal and Tsona leucogranites, outcropping respectively in the MCT hanging-wall and adjacent the STD, both crystallized at ca. 19 Ma. Their age, petrography and emplacement relations identify them as along-strike components of the HHL suite. In the central Tethyan Himalaya, the Dala granitoids are a suite of undeformed Eocene (44.1 ± 1.2 Ma) plutons emplaced into sub-greenschist facies THS metasediments. In the northern Tethyan Himalaya, the Eocene Yala-Xiangbo granitoids (42 ± 5 Ma) outcrop as part of an igneous complex in the core of the Yala-Xiangbo dome. Both the Yala-Xiangbo and Dala granitoids are significantly older than virtually all other post-collisional bodies along the main Himalayan Arc.

The thermal histories of the Yala-Xiangbo and Dala granitoids indicate that they both remained broadly isothermal from ~40 Ma until rapid exhumation at ca. 15 Ma. Because the Yala-Xiangbo complex was at significantly higher temperature than the Dala granitoids during this period, we conclude that the eastern Tethyan Himalaya was then tectonically quiescent. Exhumation of the Yala-Xiangbo complex and the Dala granitoids, was concurrent with Miocene North Himalayan Domes suggesting a structural control – probably Miocene north-directed motion on the Great Counter Thrust. Detrital zircon age-probability spectra suggest that the stratigraphy of the eastern Himalaya differs somewhat from other parts of the orogen. The Arunachal crystallines, superficially similar to the GHC, contain abundant ~800 Ma ages that are uncommon elsewhere. While our data support preservation of Paleozoic sequences in the core of the Yala-Xiangbo dome, they do not appear to be correlative with frontal-Himalayan units. Restitic granitoid zircon cores supports a local origin and/or incorporation of nearby lithologies into all of the studied east-Himalayan granitoids. However, Ti-thermometry suggests the processes of granitoid genesis are more complicated than has been recognized elsewhere.

The heat source needed to generate Eohimalayan peraluminous magmatism (and regional metamorphism) in the eastern Tethyan Himalaya is difficult to understand. Tomographic images reveal a persistent lithospheric weakness, coincident with the Ninety East Ridge, which intersects the eastern Himalaya beneath our study area. This feature may have localized heat-flow and magmatism beneath the eastern Himalaya during the Eocene.

Acknowledgements

The authors would like to thank Peter Holden for assistance with U–Th–Pb dating and development of techniques for measuring zircon Ti-content. Jim Dunlap assisted with ⁴⁰Ar/³⁹Ar thermochronology, and Trevor Ireland and Malcolm Sambridge provided advice on data-reductions and statistical data-evaluation procedures. The work was supported by funding from the Australian Research Council.

Appendix A. Supplementary material

Supplementary data associated with this article can be found, in the online version, at doi:10.1016/j.jseas.2012.01.011.

References

- Aikman, A.B., 2007. Tectonics of the Eastern Tethyan Himalaya. Ph.D. Thesis, The Australian National University.
- Aikman, A.B., Harrison, T.M., Lin, D., 2008. Evidence for early (>44 Ma) crustal thickening, Tethyan Himalaya, southeastern Tibet. *Earth Planet. Sci. Lett.* 274, 14–23.
- Ayers, J., Watson, E.B., 1991. Solubility of apatite, monazite, zircon and rutile in supercritical aqueous fluids with implications for subduction zone geochemistry. *Phil. Trans. Roy. Soc. Lond.* 335, 365–375.
- Beaumont, C., Jamieson, R.A., Nguyen, M.H., Lee, B., 2001. Himalayan tectonics explained by extrusion of a low-viscosity crustal channel coupled to focused surface denudation. *Nature* 414, 738–742.
- Beaumont, C., Jamieson, R.A., Nguyen, M.H., Medvedev, S., 2004. Crustal channel flows: 1. Numerical models with applications to the tectonics of the Himalayan–Tibetan orogen. *J. Geophys. Res.* 109, B06406.
- Burchfield, B.C., Chen, Z., Hodges, K.V., Liu, Y., Royden, L.H., Deng, C., Xu, J., 1992. The South Tibetan Detachment System, Himalayan orogen: extension contemporaneous with and parallel to shortening in a collisional mountain belt. *Geol. Soc. Am. Spec. Pap.* 269, 1–41.
- Butera, K., Williams, I., Blevin, P., Simpson, C., 2001. Zircon U–Pb dating of early Palaeozoic monzonitic intrusives from the Goonumbla area, New South Wales. *Aus. J. Earth Sci.* 48, 457–464.
- Chen, Z., Liu, Y., Hodges, K.V., Burchfiel, B.C., Royden, L.H., Deng, C., 1990. The Kangmar dome: a metamorphic core complex in southern Xizang (Tibet). *Science* 250, 1552–1556.
- Claiborne, L., Miller, C., Walker, B., Wooden, J., Mazdab, F., Bea, F., 2006. Tracking magmatic processes through Zr/Hf ratios in rocks and Hf and Ti zoning in zircons: an example from the Spirit Mountain batholith, Nevada. *Min. Mag.* 70, 517–543.
- Claiborne, L., Miller, C., Wooden, J., 2010. Trace element composition of igneous zircon: a thermal and compositional record of the accumulation and evolution of a large silicic batholith, Spirit Mountain, Nevada. *Contrib. Mineral. Petrol.* 160, 1–21.
- Claoue-Long, J., Compston, W., Roberts, J., Fanning, C., 1995. Two Carboniferous ages: a comparison of SHRIMP zircon dating with conventional zircon ages and $^{40}\text{Ar}/^{39}\text{Ar}$ analysis. *Soc. Sed. Geol. Spec. Pap.* 54, 3–21.
- Copeland, P., Harrison, T.M., Le Fort, P., 1990. Age and cooling history of the Manaslu Granite – implications for Himalayan tectonics. *J. Volc. Geotherm. Res.* 44, 33–50.
- Cumming, G., Richards, J., 1975. Ore lead isotope ratios in a continuously changing earth. *Earth Planet. Sci. Lett.* 28, 155–171.
- Davis, J.H., von Blanckenburg, F., 1995. Slab breakoff: a model of lithosphere detachment and its test in the magmatism and deformation of collisional orogens. *Earth Planet. Sci. Lett.*, 85–102.
- Debon, F., Le Fort, P., Sheppard, S., Sonet, J., 1986. The four plutonic belts of the Transhimalaya–Himalaya: a chemical, mineralogical, isotopic, and chronological synthesis along a Tibet–Nepal granite section. *J. Petrol.* 27, 219–250.
- DeCelles, P.G., Robinson, D.M., Quade, J., Copeland, P., Upreti, B.N., Ojha, T.P., Garzione, C.N., 2001a. Regional structure and stratigraphy of the Himalayan fold-thrust belt, far western Nepal. *Tectonics* 20, 487–509.
- DeCelles, P.G., Robinson, D.M., Quade, J., Ojha, T.P., Garzione, C.N., Copeland, P., Upreti, B.N., 2001b. Stratigraphy, structure, and tectonic evolution of the Himalayan fold-thrust belt in western Nepal. *Tectonics* 20 (4), 487–509.
- Deniel, C., Vidal, P., Fernandez, A., Le Fort, P., Peucat, J., 1987. Isotopic study of the Manaslu Granite (Himalaya, Nepal) – inferences on the age and source of Himalayan leucogranites. *Contrib. Min. Petrol.* 96, 78–92.
- Ding, L., Kapp, P., Wan, X., 2005. Paleocene–Eocene record of ophiolite obduction and initial India–Asia collision, south central Tibet. *Tectonics*, 24, TC3001. doi:10.1029/2004TC001729.
- Edwards, M.A., Harrison, T.M., 1997. When did the roof collapse? Late Miocene north-south extension in the High Himalaya revealed by Th–Pb Monazite dating of the Khula Kangri Granite. *Geology* 25, 543–546.
- England, P., Le Fort, P., Molnar, P., Pecher, A., 1992. Heat sources for Tertiary magmatism and anatexis in the Annapurna–Manaslu region of central Nepal. *J. Geophys. Res.* 97, 2107–2128.
- Ferry, J.M., Watson, E.B., 2007. New thermodynamic models and revised calibrations for the Ti-in-zircon and Zr-in-rutile thermometers. *Contrib. Min. Petrol.* 154, 429–437.
- Francheteau, J., Jaupart, C., Jie, S.X., Hua, K.W., Lu, L.D., Chi, B.J., Pin, W.H., Yeu, D.H., 1984. High heat flow in southern Tibet. *Nature* 307, 32–36.
- Gansser, A., 1964. *The Geology of the Himalayas*. Wiley Interscience, New York, 289p.
- Gehrels, G.E., DeCelles, P.G., Martin, A., Ojha, T.P., Pinhasi, G., Upreti, B.N., 2003. Initiation of the Himalayan orogen as an early Paleozoic thin-skinned thrust belt. *GSA Today* 13, 4–10.
- Guillot, S., Hodges, K.V., Le Fort, P., Pecher, A., 1994. New constraints on the age of the Manaslu Leucogranite; evidence for episodic tectonic denudation in the central Himalayas. *Geology* 22, 559–562.
- Harris, N., Inger, S., 1992. Trace element modelling of pelite-derived granites. *Contrib. Min. Petrol.* 110, 46–56.
- Harris, N., Massey, J., 1994. Decompression and anatexis of Himalayan metapelites. *Tectonics* 13, 1537–1546.
- Harrison, T.M., Watson, E.B., 1983. Kinetics of zircon dissolution and zirconium diffusion in granitic melts of variable water-content. *Contrib. Mineral. Petrol.* 84, 66–72.
- Harrison, T.M., Aleinikoff, J.N., Compston, W., 1987. Observations and controls on the occurrence of inherited zircons in Concord-type granitoids, New Hampshire. *Geochim. Cosmochim. Acta* 51, 2549–2558.
- Harrison, T.M., McKeegan, K.D., Le Fort, P., 1995. Detection of inherited monazite in the Manaslu Leucogranite by Pb-208/Th-232 ion microprobe dating – crystallization age and tectonic implications. *Earth Planet. Sci. Lett.* 133, 271–282.
- Harrison, T.M., Lovera, O.M., Grove, M., 1997. New insights into the origin of two contrasting Himalayan granite belts. *Geology* 25, 899–902.
- Harrison, T.M., Grove, M., Lovera, O.M., Catlos, E.J., 1998. A model for the origin of Himalayan anatexis and inverted metamorphism. *J. Geophys. Res.* 103 (27), 017–27, 032.
- Harrison, T.M., Grove, M., McKeegan, K.D., Coath, C.D., Lovera, O.M., Le Fort, P., 1999. Origin and episodic emplacement of the Manaslu intrusive complex, central Himalaya. *J. Petrol.* 40, 3–19.
- Harrison, T.M., Yin, A., Grove, M., Lovera, O.M., Ryerson, F.J., 2000. The Zedong Window: A record of superposed Tertiary convergence in southeastern Tibet. *J. Geophys. Res.* 105, 19,211–19,230.
- Harrison, T.M., Catlos, E.J., Montel, J., 2002. U–Th–Pb dating of phosphate minerals. *Revs. Mineral. Geochem. Phosphates, Mineral. Soc. Am.* 48, 523–558.
- Harrison, T.M., Watson, E.B., Aikman, A.B., 2007. Temperature spectra of zircon crystallization in plutonic rocks. *Geology* 35, 635–638.
- Harrison, T.M., Celerier, J., Aikman, A.B., Hermann, J., Heizler, M.T., 2009. Diffusion of ^{40}Ar in muscovite. *Geochim. Cosmochim. Acta* 73 (4), 1051–1092.
- Hermann, J., Rubatto, D., Trommsdorff, V., 2006. Sub-solidus Oligocene zircon formation in garnet peridotite during fast decompression and fluid infiltration (Duria, central Alps). *Mineral. Petrol.* 88, 181–206.
- Hu, S., He, L., Wang, J., 2000. Heat flow in the continental area of China: a new data set. *Earth Planet. Sci. Lett.* 179, 407–419.
- Huang, W.L., Wyllie, P.J., 1986. Phase relationships of gabbro–tonalite–granite–water at 15 kbar with applications to differentiation and anatexis. *Am. Min.* 71, 301–316.
- Inger, S., Harris, N., 1993. Geochemical constraints on leucogranite magmatism in the Langtang valley, Nepal Himalaya. *J. Petrol.* 34, 345–368.
- Jamieson, R., Beaumont, C., Medvedev, S., Nguyen, M., 2004. Crustal channel flows: 2. Numerical models with implications for metamorphism in the Himalayan–Tibetan orogen. *J. Geophys. Res.* 109, B06407.
- Kennett, B., Widiyantoro, S., 1999. A low seismic wavespeed anomaly beneath northwestern India: a seismic signature of the Deccan plume? *Sci. Lett.* 165, 145–155.
- Kennett, B., Widiyantoro, S., van der Hilst, R., 1998. Joint seismic tomography for bulk sound and shear wave speed in the Earth’s mantle. *J. Geophys. Res.* 103, 12469–12494.
- King, J., Harris, N., Argles, T., Parrish, R.R., Zhang, H., 2011. Contribution of crustal anatexis to the tectonic evolution of Indian crust beneath southern Tibet. *Geol. Soc. Am. Bull.* 123, 218–239.
- Le Fort, P., 1975. Himalayas, the collided range. Present knowledge of the continental arc. *Am. J. Sci.* 275 (A), 1–44.
- Le Fort, P., 1996. Evolution of the Himalaya. In: Yin, A., Harrison, T.M. (Eds.), *The Tectonics of Asia*. Cambridge University Press, pp. 95–106.
- Le Fort, P., Vuney, M., Deniel, C., France-Lanord, C., 1987. Crustal generation of the Himalayan leucogranites. *Tectonophysics* 134, 39–57.
- Lee, J., Hacker, B.R., Dinklage, W.S., Wang, Y., Gans, P., Calvert, A., Wan, J.L., Chen, W.J., Blythe, A.E., McClelland, W., 2000. Evolution of the Kangmar Dome, southern Tibet: structural, petrologic, and thermochronologic constraints. *Tectonics* 19, 872–895.
- Lee, J., Hacker, B., Wang, Y., 2004. Evolution of North Himalayan Gneiss Domes: Structural and metamorphic studies in Mabja Dome, southern Tibet. *J. Struct. Geol.* 26, 2297–2316.
- Lovera, O.M., Richter, F.M., Harrison, T.M., 1989. The $^{40}\text{Ar}/^{39}\text{Ar}$ thermochronometry for slowly cooled samples having a distribution of diffusion domain sizes. *J. Geophys. Res.* 94, 17917–17936.
- Ludwig, K., 2001. *Squid 1.02: A User Manual*. Berkeley Geochronological Center Spec. Pub. 2, p. 19.
- McDougall, I., Harrison, T.M., 1999. *Geochronology and Thermochronology by the $^{40}\text{Ar}/^{39}\text{Ar}$ Method*. Oxford University Press.
- Mo, X., Zhao, Z., Deng, J., Flower, M., Yu, X., Luo, Z., Li, Y., Zhou, S., Dong, G., Zhu, D., Wang, L., 2006. Petrology and geochemistry of postcollisional volcanic rocks from the Tibetan plateau: implications for lithosphere heterogeneity and collision induced asthenospheric mantle flow. In: Dilek, Y., Pavlides, S. (Eds.), *Postcollisional Tectonics and Magmatism in the Mediterranean Region and Asia*. *Geol. Soc. Am. Spec. Pap.* 409, 507–530.
- Mo, X.X., Niu, Y.L., Dong, G.C., Zhao, Z., Hou, Z., Zhou, S., Ke, S., 2008. Contribution of syncollisional felsic magmatism to continental crust growth: a case study of the Paleogene Linzizong volcanic Succession in southern Tibet. *Chem. Geol.* 250, 49–67.
- Myrow, P.M., Hughes, N.C., Paulsen, T.S., Williams, I.S., Parcha, S.K., Thompson, K.R., Bowring, S.A., Peng, S.C., Ahluwalia, A.D., 2003. Integrated tectonostratigraphic analysis of the Himalaya and implications for its tectonic reconstruction. *Earth Planet. Sci. Lett.* 212, 433–441.
- Nelson, K.D., Zhao, W.J., Brown, L.D., et al., 1996. Partially molten middle crust beneath southern Tibet: synthesis of project indepth results. *Science* 274, 1684–1688.
- Paces, J., Miller, J., 1993. U–Pb ages of Duluth complex and related mafic intrusions, northeastern Minnesota: geochronological insights to physical, petrogenetic, palaeomagnetic, and tectonomagmatic processes associated with the 1.1 Ga mid-continent rift system. *J. Geophys. Res.* 98, 13997–14013.

- Pan, G., Ding, J., Yao, D., Wang, L., 2004. Geological map of Qinghai-Xiang (Tibet) Plateau and Adjacent Areas (1:1500,000). China Geological Survey, Chengdu Cartographic Publishing House, Chengdu, China.
- Pinet, C., Jaupart, C., 1987. A thermal model for the distribution in space and time of the Himalayan granites. *Earth Planet. Sci. Lett.* 84, 87–99.
- Press, W.H., Teukolsky, S.A., Vetterling, W.T., Flannery, B.P., 1992. *Numerical Recipes in FORTRAN. The Art of Scientific Computing*, second ed. University Press, Cambridge.
- Prince, C.P., Harris, N., Vance, D., 2001. Fluid enhanced melting during prograde metamorphism. *J. Geol. Soc. Lond.* 158, 233–241.
- Pullen, A., Kapp, P., DeCelles, P.G., Gehrels, G.E., Ding, L., 2011. Cenozoic anatexis and exhumation of Tethyan Sequence rocks in the Xiao Gurla Range, Southwest Tibet. *Tectonophysics* 501, 28–40.
- Quigley, M., Liangjun, Y., Xiaohan, L., Wilson, C.J.L., Sandiford, M., Phillips, D., 2006. $^{40}\text{Ar}/^{39}\text{Ar}$ thermochronology of the Kampa dome, southern Tibet: Implications for tectonic evolution of the North Himalayan gneiss domes. *Tectonophysics* 421, 268–297.
- Quigley, M.C., Liangjun, Y., Gregory, C., Corvino, A., Sandiford, M., Wilson, C.J.L., Xiaohan, L., 2008. U–Pb SHRIMP zircon geochronology and T–t history of the Kampa dome, southern Tibet. *Tectonophysics* 446, 97–113.
- Ratschbacher, L., Frisch, W., Liu, G., Chen, C.C., 1994. Distributed deformation in southern and western Tibet during and after the India–Asia collision. *J. Geophys. Res.* 99 (19), 917–919, 945.
- Renne, P.R., Swisher, C.C., Deino, A.L., Karner, D.B., Owens, T.L., DePaolo, D.J., 1998. Intercalibration of standards, absolute ages and uncertainties in $^{40}\text{Ar}/^{39}\text{Ar}$ dating. *Chem. Geol.* 145, 117–152.
- Scharer, U., 1984. The effect of initial ^{230}Th disequilibrium on young U–Pb ages: the Makalu case, Himalayas. *Earth Planet. Sci. Lett.* 99, 19817–19945.
- Scharer, U., Ronghua, X., Allègre, C., 1986. U–(Th)–Pb systematics and ages of Himalayan leucogranites, south Tibet. *Earth Planet. Sci. Lett.* 77, 35–48.
- Simons, F., Zielhuis, A., van der Hilst, R., 1999. The deep structure of the Australian continent from surface wave tomography. *Lithos* 48, 7–43.
- Singh, S., 2003. Conventional and SHRIMP U–Pb zircon dating of the Chor granitoid, Himachal Himalaya. *J. Geol. Soc. Ind.* 62, 614–626.
- Steiger, R.H., Jäger, E., 1977. Submission on geochronology – convention on use of decay constants in geochronology and cosmochronology. *Earth Planet. Sci. Lett.* 36 (3), 359–362.
- Tetley, N., McDougall, I., Heydegger, H., 1980. Thermal neutron interferences in the $^{40}\text{Ar}/^{39}\text{Ar}$ dating technique. *J. Geophys. Res.* 85, 7201–7205.
- Townsend, K.J., Miller, C.F., D'Andrea, J.L., Ayers, J.C., Harrison, T.M., Coath, C.D., 2000. Low temperature replacement of monazite in the Ireteba granite, Southern Nevada: geochronological implications. *Chem. Geol.* 172, 95–112.
- Wang, Y., 2000. Active Deformation Style in South-eastern and North Margins of Tibetan plateau. *Earth Science Frontiers* 7, Abstract Volume of the 15th Himalaya–Karakorum–Tibet, Workshop, p. 267.
- Wang, Y., 2001. Heat flow pattern and lateral variations of lithosphere strength in China mainland: constraints on active deformation. *Phys. Earth Planet. Int.* 126, 121–146.
- Watson, E.B., 1996. Dissolution, growth and survival of zircons during crustal fusion: kinetic principles, geological models and implications for isotopic inheritance. *Geol. Soc. Am. Spec. Pap.* 315, 43–56.
- Watson, E.B., Harrison, T.M., 1983. Zircon saturation revisited: Temperature and composition effects in a variety of crustal magma types. *Earth Planet. Sci. Lett.* 64, 295–304.
- Watson, E.B., Harrison, T.M., 2005. Zircon thermometer reveals minimum melting conditions on earliest earth. *Science* 308 (5723), 841–844.
- Watson, E.B., Wark, D.A., Thomas, J.B., 2006. Crystallization thermometers for zircon and rutile. *Contrib. Min. Petrol.* 151, 413–433.
- Williams, I.S., 1998. U–Th–Pb geochronology by ion microprobe. In: McKibben, M.A., W.C.S., Ridley, W.I. (Eds.), *Applications of Microanalytical Techniques to Understanding Mineralizing Processes*. *Revs. Econ. Geol.* 7, pp. 1–35.
- Williams, I., Hergt, J., 2000. U–Pb dating of Tasmanian dolerites: A cautionary tale of SHRIMP analysis of high-U zircon. In: Woodhead, J., Hergt, J., Noble, W. (Eds.), *Beyond 2000: New Frontiers in Isotope Geoscience* Lorne.
- Yin, A., 2006. Cenozoic evolution of the Himalayan orogen as constrained by along-strike variations of structural geometry, exhumation history, and foreland sedimentation. *Earth Sci. Rev.* 76, 1–134.
- Yin, A., Harrison, T.M., 2000. Geologic evolution of the Himalayan–Tibetan orogen. *Ann. Rev. Earth. Planet. Sci.* 28, 211–280.
- Yin, A., Harrison, T.M., Ryerson, F.J., Wenji, C., Kidd, W.S.F., Copeland, P., 1994. Tertiary structural evolution of the Gangdese Thrust system, southeastern Tibet. *J. Geophys. Res.* 99, 18175–18201.
- Zeng, L., Gao, L.E., Xie, K., Zeng, J.L., 2011. Mid-Eocene high Sr/Y granites in the Northern Himalayan Gneiss Domes: melting thickened lower continental crust. *Earth Planet. Sci. Lett.* 303, 251–266.
- Zhang, H.F., Harris, N., Parrish, R., Kelley, S., Zhang, L., Rogers, N., Argles, T., King, J., 2004a. Causes and consequences of protracted melting of the mid-crust exposed in the North Himalayan Antiform. *Earth Planet. Sci. Lett.* 228, 195–212.
- Zhang, H.F., Harris, N., Parrish, R., Zhang, L., Zhao, Z., 2004b. U–Pb ages of Kude And Sajia leucogranites in Saffia Dome from North Himalaya and their geological implications. *Chin. Sci. Bull.* 49, 2087–2092.